

SDE-Driven Spatio-Temporal Hypergraph Neural Networks for Irregular Longitudinal fMRI Connectome Modeling in Alzheimer’s Disease

Ruiying Chen^{1*}, Yutong Wang^{2*}, Houliang Zhou¹, Wei Liang¹, Yong Chen, MD, PhD³,
Lifang He, PhD¹

¹ Lehigh University, Bethlehem, PA, USA

² New York University, New York, NY, USA

³ University of Pennsylvania, Philadelphia, PA, USA

Abstract

Longitudinal neuroimaging is essential for modeling disease progression in Alzheimer’s disease (AD), yet irregular sampling and missing visits pose substantial challenges for learning reliable temporal representations. To address this challenge, we propose SDE-HGNN, a stochastic differential equation (SDE)-driven spatio-temporal hypergraph neural network for irregular longitudinal fMRI connectome modeling. The framework first employs an SDE-based reconstruction module to recover continuous latent trajectories from irregular observations. Based on these reconstructed representations, dynamic hypergraphs are constructed to capture higher-order interactions among brain regions over time. To further model temporal evolution, hypergraph convolution parameters evolve through SDE-controlled recurrent dynamics conditioned on inter-scan intervals, enabling disease-stage-adaptive connectivity modeling. We also incorporate a sparsity-based importance learning mechanism to identify salient brain regions and discriminative connectivity patterns. Extensive experiments on the OASIS-3 and ADNI cohorts demonstrate consistent improvements over state-of-the-art graph and hypergraph baselines in AD progression prediction. The source code is available at <https://anonymous.4open.science/r/SDE-HGNN-017F>.

Introduction

Alzheimer’s disease (AD) is a progressive neurodegenerative disorder characterized by gradual cognitive decline and widespread disruption of brain networks. Because neuropathological changes unfold over many years before clinical diagnosis, accurately modeling disease progression is essential for early detection and prognosis prediction¹. Longitudinal neuroimaging provides repeated observations of brain function over time and offers unique opportunities to characterize subject-specific disease trajectories and heterogeneous progression patterns.

Resting-state functional magnetic resonance imaging (rs-fMRI) enables the study of functional connectivity among distributed brain regions and has been widely used to investigate network-level alterations associated with AD^{2,3}. However, longitudinal neuroimaging data collected in clinical cohorts are inherently irregular: visits are unevenly spaced, follow-up intervals vary substantially across subjects, and missing observations frequently occur. Importantly, such irregularity arises at two temporal scales. (1) *within-scan level*, where ROI-level fMRI time series may contain noisy, incomplete, or corrupted observations due to motion artifacts or signal instability, potentially affecting the estimation of functional connectivity; and (2) *across-visit level*, where longitudinal imaging visits occur at irregular time intervals and may be missing entirely for some subjects, making it difficult to model disease progression using discrete-time approaches. These characteristics pose significant challenges for conventional machine learning methods to learn reliable temporal representations of disease progression from irregular longitudinal data.

Graph neural networks (GNNs) have demonstrated strong potential for modeling brain connectivity by learning structured representations from functional connectomes^{4,5,6}. In these approaches, brain networks are typically represented as graphs where nodes correspond to brain regions and edges encode pairwise functional connectivity between regions. Despite recent advances, two fundamental limitations remain when applying existing GNN-based approaches to irregular longitudinal fMRI connectomes. First, most existing models rely on discrete-time architectures or fixed temporal grids, which are not well suited to heterogeneous follow-up intervals and missing visits. As a result, temporal dynamics may be inaccurately represented when observations occur at irregular time points. Recent studies have

*These authors contributed equally.

explored ordinary differential equation (ODE)- or stochastic differential equation (SDE)-based frameworks for modeling continuous-time dynamics of longitudinal brain networks under irregular sampling^{7,8,9}. While these approaches improve temporal modeling, they typically rely on pairwise graph representations. Second, conventional graph representations assume pairwise relationships between brain regions. However, many cognitive and pathological processes arise from coordinated activity among multiple regions simultaneously. Consequently, modeling brain networks using only pairwise edges may provide an incomplete description of higher-order functional organization.

Hypergraphs provide a natural extension of conventional graphs by allowing each hyperedge to connect multiple nodes simultaneously, enabling explicit modeling of coordinated multi-region interactions in brain networks. Although hypergraph neural networks have been explored for brain connectome analysis (e.g., DwHGNCN¹⁰, HyperGALE¹¹, HGST¹²), most existing methods focus on spatial connectivity modeling under static-time assumptions. Some recent studies extend hypergraph learning to longitudinal settings. For example, Hao et al.¹³ proposed a weighted hypergraph convolutional network (WHGNCN) for longitudinal AD analysis by constructing hypergraphs at each time point and fusing them through weighted aggregation. However, this approach models relationships between subjects rather than between brain regions, and relies on discrete-time fusion across predefined visits. Consequently, existing hypergraph-based approaches cannot jointly model continuous-time disease progression and higher-order brain network interactions in irregular longitudinal neuroimaging data.

To address these limitations, we propose SDE-HGNN, an SDE-driven spatio-temporal hypergraph neural network for irregular longitudinal fMRI connectome modeling. The proposed framework integrates continuous-time modeling with higher-order brain network representation to capture both temporal disease dynamics and coordinated multi-region functional interactions. Specifically, we first employ an SDE-based module to reconstruct ROI-level fMRI signals as continuous stochastic trajectories, mitigating the effects of irregular or incomplete observations. Based on the reconstructed representations, we construct dynamic hypergraphs that model higher-order relationships among multiple brain regions. To model longitudinal disease progression, hypergraph convolution parameters are further evolved through SDE-controlled recurrent dynamics conditioned on inter-visit intervals. In addition, we incorporate a sparsity-based importance learning mechanism to identify salient brain regions and discriminative connectivity patterns associated with AD progression. SDE-HGNN is the first framework that jointly models continuous-time longitudinal dynamics and higher-order brain network interactions for irregular fMRI connectome analysis.

The main contributions of this work are summarized as follows:

- We introduce an SDE-based reconstruction module to model ROI-level fMRI signals as continuous stochastic trajectories, addressing irregular or incomplete observations in fMRI time series.
- We develop a novel SDE-guided spatio-temporal hypergraph neural network in which hypergraph convolution parameters evolve continuously according to inter-visit intervals, enabling adaptive modeling of disease progression under irregular longitudinal sampling.
- We incorporate a sparsity-based learning mechanism within the hypergraph framework to identify salient brain regions and disease-specific connectivity patterns, providing interpretable insights into AD progression.
- Extensive experiments on the OASIS-3 and ADNI cohorts demonstrate consistent improvements over state-of-the-art graph and hypergraph baselines while revealing clinically meaningful longitudinal connectivity biomarkers aligned with known AD pathology.

Methodology

We consider the problem of predicting disease progression from irregular longitudinal rs-fMRI connectomes. Suppose that each subject contains multiple imaging visits acquired at irregular time intervals. For a subject with up to T visits occurring at time points $\{t_1, t_2, \dots, t_T\}$, the inter-visit interval is defined as $\Delta t_k = t_k - t_{k-1}$. For each visit, ROI-level BOLD time series are extracted after standard preprocessing and brain parcellation. Let N denote the number of regions of interest (ROIs) and D the feature dimension per ROI. After preprocessing, the ROI feature matrix at visit t_k is denoted by $\mathbf{X}_{t_k} \in \mathbb{R}^{N \times D}$, where each row corresponds to the feature representation of one brain region. As discussed in the Introduction, irregularity in longitudinal rs-fMRI arises at two temporal scales: noisy or incomplete ROI time series within scans and heterogeneous intervals between visits. To address these challenges, our proposed

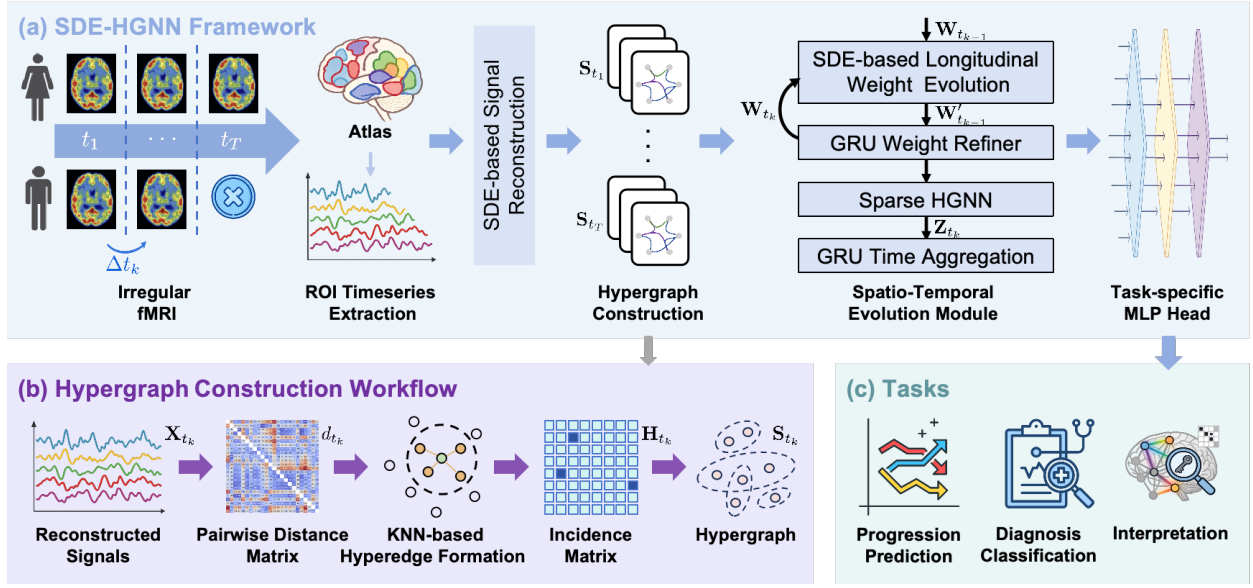


Figure 1. Overview of SDE-HGNN framework. (a) Irregular longitudinal fMRI signals are reconstructed using a neural SDE, followed by hypergraph construction and SDE-driven spatio-temporal modeling with GRU refinement and aggregation. (b) Hypergraph construction from reconstructed ROI signals via pairwise distance computation and KNN-based hyperedge formation. (c) Downstream tasks include progression prediction, diagnosis classification and interpretation.

SDE-HGNN framework consists of three sequential stages: (1) SDE-based fMRI signal reconstruction, (2) hypergraph construction at each visit, and (3) SDE-guided spatio-temporal hypergraph modeling. An overview of the SDE-HGNN framework is shown in Fig. 1.

SDE-based fMRI Signal Reconstruction. Resting-state fMRI signals are inherently noisy and may contain irregular or incomplete observations. To obtain temporally coherent ROI-level representations, we model each ROI’s BOLD time series as a continuous stochastic process. Specifically, we adopt a neural stochastic differential equation (SDE) encoder–decoder framework¹⁴. A recurrent neural network (RNN) encoder first processes the irregularly sampled observations and maps them to an approximate posterior over an initial latent state \mathbf{z}_0 . A neural SDE then models the latent trajectory as

$$d\mathbf{z}_t = f_\theta(\mathbf{z}_t, t) dt + g_\theta(\mathbf{z}_t, t) dB_t \quad (1)$$

where t denotes continuous time within a scan, f_θ is a neural network–parameterized drift function modeling deterministic temporal dynamics, g_θ is a learnable diffusion function controlling stochastic variability in the latent process, and B_t denotes standard Brownian motion.

The learned SDE enables interpolation at arbitrary time points, generating continuous latent trajectories \mathbf{z}_t even under irregular sampling. A decoder then reconstructs complete ROI-level time series from these latent states. This reconstruction step mitigates artifacts caused by irregular intra-scan sampling and ensures that downstream functional connectivity estimation is based on temporally consistent signals. After reconstruction, each visit t_k is represented by an ROI feature matrix $\mathbf{X}_{t_k} \in \mathbb{R}^{N \times D}$.

Hypergraph Construction. Standard connectome modeling constructs pairwise connectivity graphs via ROI-ROI correlations. However, many neural processes arise from coordinated activity among multiple brain regions simultaneously. To explicitly model such higher-order interactions, we construct a hypergraph at each visit, which generalizes the standard graph by allowing each hyperedge to connect an arbitrary subset of nodes. For each hypernode v_i , we compute pairwise Euclidean distances between node features and select its K -nearest neighbors (KNN) to form a

hyperedge e_j .

Let $\mathbf{x}_{t_k}^{(i)} \in \mathbb{R}^D$ denote the feature vector of ROI i , corresponding to the i -th row of \mathbf{X}_{t_k} . The hypergraph incidence matrix at visit t_k is defined as

$$H_{t_k}(i, j) = \begin{cases} \exp\left(-\frac{d_{t_k}^{(ij)^2}}{(q \cdot \bar{d}_{t_k}^{(i)})^2}\right), & v_i \in \mathcal{N}_K(v_i) \\ 0, & \text{otherwise} \end{cases} \quad (2)$$

where $d_{t_k}^{(ij)} = \|\mathbf{x}_{t_k}^{(i)} - \mathbf{x}_{t_k}^{(j)}\|_2$ and $\bar{d}_{t_k}^{(i)}$ denotes the mean distance from hypernode v_i to all other hypernodes, q is a scaling parameter, and $\mathcal{N}_K(v_i)$ denotes the K -nearest-neighbor set of hypernode v_i . Each hypernode participates in multiple overlapping hyperedges, enabling message passing beyond pairwise relationships.

Let $\mathbf{M}_e = \text{diag}(m_1, \dots, m_E) \in \mathbb{R}^{E \times E}$ denote the diagonal hyperedge weight matrix, where m_j is the weight of hyperedge e_j (initialized to 1 and later modulated by learned importance probabilities), and E denotes the number of hyperedges. Hypernode degrees and hyperedge degrees are defined as

$$d(v_i) = \sum_{j=1}^E m_j H_{t_k}(i, j), \quad \delta(e_j) = \sum_{i=1}^N H_{t_k}(i, j). \quad (3)$$

Let $\mathbf{D}_v \in \mathbb{R}^{N \times N}$ and $\mathbf{D}_e \in \mathbb{R}^{E \times E}$ denote the diagonal hypernode and hyperedge degree matrices. The normalized hypergraph propagation matrix can be expressed as

$$\mathbf{S}_{t_k} = \mathbf{D}_v^{-1/2} \mathbf{H}_{t_k} \mathbf{M}_e \mathbf{D}_e^{-1} \mathbf{H}_{t_k}^T \mathbf{D}_v^{-1/2}. \quad (4)$$

The propagation matrix \mathbf{S}_{t_k} encodes higher-order neighborhood relationships for downstream hypergraph convolution.

SDE-guided Spatio-temporal HGNN. To model longitudinal disease progression under irregular visit intervals, we allow the hypergraph convolution parameters to evolve continuously over time. Let $\mathbf{W}_{t_k} \in \mathbb{R}^{D \times d_l}$ denote the hypergraph convolution weight state at visit t_k , where d_l is the number of output dimensions. We model its evolution as an SDE-driven continuous-time stochastic process

$$\mathbf{W}'_{t_k} = \text{SDEsolve}(f_\theta, \mathbf{W}_{t_{k-1}}, \Delta t_k), \quad (5)$$

where f_θ is a learnable drift function and Δt_k is the inter-visit time interval.

To incorporate visit-specific information, we further refine the evolved weights using a gated recurrent unit (GRU) module conditioned on the current ROI features:

$$\mathbf{W}_{t_k} = \text{GRU}(\mathbf{X}_{t_k}, \mathbf{W}'_{t_k}) + \text{GRU}(\mathbf{X}_{t_k}, \mathbf{W}_0), \quad (6)$$

where the second term introduces a time-invariant baseline initialized by a learnable weight state \mathbf{W}_0 shared across visits, allowing the convolution parameters to adapt dynamically to heterogeneous disease progression rates.

The refined weight matrix \mathbf{W}_{t_k} is then used in the hypergraph convolution operator to compute visit-specific hypernode representations:

$$\mathbf{Z}_{t_k} = \sigma(\mathbf{S}_{t_k} \mathbf{X}_{t_k} \mathbf{W}_{t_k}), \quad (7)$$

where $\mathbf{Z}_{t_k} \in \mathbb{R}^{N \times d_l}$ is the output hypernode embeddings, and σ is the activation function. Through this process, the model captures higher-order interactions among brain regions while jointly modeling continuous-time disease progression in irregular longitudinal neuroimaging data.

Sparse Interpretability. The hypergraph structure \mathbf{S}_{t_k} and hypernode feature matrix \mathbf{X}_{t_k} may contain redundant or noisy information that is not essential for disease prediction. To identify informative brain regions and connectivity patterns, we introduce a sparsity-based interpretability mechanism that learns importance scores for both hypernode features and hyperedges. Specifically, inspired by GNNExplainer¹⁵, we learn the hypernode feature importance probabilities $\mathbf{P}_X \in \mathbb{R}^{N \times D}$ and hyperedge importance probabilities $\mathbf{P}_E \in \mathbb{R}^E$. The sparsified hypernode features are obtained by

$$\tilde{\mathbf{X}}_{t_k} = \mathbf{X}_{t_k} \odot \mathbf{P}_X, \quad (8)$$

where \odot denotes the element-wise multiplication.

Let $\mathbf{P}_E = [p_{E_1}, p_{E_2}, \dots, p_{E_N}]$ denote the vector of hyperedge importance probabilities, where p_{E_i} represents the importance score of hyperedge e_i . Each hyperedge importance probability is computed from the importance-weighted feature of its center node:

$$p_{E_i} = \sigma(\mathbf{v}^\top (\mathbf{x}_{t_k}^{(i)} \odot \mathbf{p}_i)), \quad (9)$$

where $\mathbf{v} \in \mathbb{R}^D$ is a learnable projection vector, and $\mathbf{p}_i \in \mathbb{R}^D$ is the i -th row of the hypernode feature importance matrix \mathbf{P}_X , corresponding to the feature importance weights of hypernode i .

Using these learnable importance probabilities, the hypergraph propagation matrix is recomputed as

$$\tilde{\mathbf{S}}_{t_k} = \tilde{\mathbf{D}}_v^{-1/2} \mathbf{H}_{t_k} \text{diag}(p_{E_1}, \dots, p_{E_N}) \tilde{\mathbf{D}}_e^{-1} \mathbf{H}_{t_k}^\top \tilde{\mathbf{D}}_v^{-1/2}, \quad (10)$$

Finally, the sparsified hypernode representations are computed as

$$\hat{\mathbf{Z}}_{t_k} = \sigma(\tilde{\mathbf{S}}_{t_k} \tilde{\mathbf{X}}_{t_k} \mathbf{W}_{t_k}). \quad (11)$$

which replaces the original convolution in Eq. (7). This sparsification mechanism enables the model to identify salient brain regions and discriminative connectivity patterns associated with disease progression.

Loss Function. After hypergraph convolution, node embeddings $\hat{\mathbf{Z}}_{t_k}$ are aggregated via global max and mean pooling to obtain graph-level representations. The resulting features are fed to a multilayer perceptron (MLP) classifier for disease progression prediction. The overall training objective combines classification loss with sparsity and information-preserving regularization:

$$\mathcal{L} = \mathcal{L}_{ce} + \lambda_1 \mathcal{L}_{mi} + \lambda_2 \mathcal{L}_s + \lambda_3 \mathcal{L}_e. \quad (12)$$

The classification loss is defined as

$$\mathcal{L}_{ce} = -(y \log \sigma(\hat{y}) + (1 - y) \log(1 - \sigma(\hat{y}))). \quad (13)$$

To ensure that the sparsified hypernode features and hypergraph structure preserve sufficient predictive information, we introduce a mutual information regularization term

$$\mathcal{L}_{mi} = - \sum_{c=1}^C \mathbb{1}[y = c] \log P_{\Phi}(\hat{y} = y \mid \tilde{\mathbf{S}}_{t_k}, \tilde{\mathbf{X}}_{t_k}), \quad (14)$$

which maximizes the mutual information between the sparsified representations and the disease labels.

The sparsity regularization is defined as

$$\mathcal{L}_s = \|\mathbf{P}_X\|_1 + \frac{1}{T} \sum_{k=1}^T \|\mathbf{P}_E\|_1. \quad (15)$$

To encourage discrete feature selection, we further apply binary entropy regularization: $\mathcal{L}_e = \mathcal{L}_{P_X} + \mathcal{L}_{P_E}$, where

$$\mathcal{L}_{P_X} = -(\mathbf{P}_X \log(\mathbf{P}_X) + (1 - \mathbf{P}_X) \log(1 - \mathbf{P}_X)), \quad \mathcal{L}_{P_E} = -\frac{1}{T} \sum_{k=1}^T (\mathbf{P}_E \log(\mathbf{P}_E) + (1 - \mathbf{P}_E) \log(1 - \mathbf{P}_E)). \quad (16)$$

Together, these losses encourage the model to identify a compact subset of salient ROIs and hyperedges that are most informative for predicting disease progression. The coefficients λ_1 , λ_2 , and λ_3 are tunable hyperparameters that control the trade-off among the different loss terms.

Table 1. Classification comparisons for stable vs. progressive subjects on OASIS-3.

Num. of Timepoints	Methods	AUC	Accuracy	Sensitivity	Specificity
Cross-sectional	DGCNN	0.6812 ± 0.0094	0.6500 ± 0.0240	0.6246 ± 0.0946	0.6587 ± 0.0629
	DwHGNCN	0.6168 ± 0.0346	0.6988 ± 0.0095	0.3275 ± 0.1117	0.8286 ± 0.0428
	HyperGALE	0.6408 ± 0.0483	0.6614 ± 0.0150	0.4365 ± 0.0094	0.7250 ± 0.0280
	HGST	0.6348 ± 0.0516	0.7162 ± 0.0230	0.5707 ± 0.0368	0.8718 ± 0.0195
1	BrainTokenGT	0.4840 ± 0.0403	0.5369 ± 0.2150	0.3853 ± 0.4239	0.5874 ± 0.4364
	WHGNCN	0.5539 ± 0.0748	0.5292 ± 0.1390	0.5278 ± 0.2461	0.5292 ± 0.2613
	SDEGCN	0.5702 ± 0.0598	0.6706 ± 0.0706	0.2385 ± 0.1122	0.8213 ± 0.1323
	SDE-HGNN	0.6067 ± 0.0458	0.7148 ± 0.0460	0.2324 ± 0.1575	0.8825 ± 0.0905
2	BrainTokenGT	0.5230 ± 0.0252	0.5061 ± 0.0547	0.5480 ± 0.1240	0.4912 ± 0.1085
	WHGNCN	0.5848 ± 0.0690	0.5967 ± 0.1482	0.5457 ± 0.2451	0.6155 ± 0.2749
	SDEGCN	0.6738 ± 0.0396	0.6236 ± 0.1818	0.5865 ± 0.2165	0.6374 ± 0.3173
	SDE-HGNN	0.7293 ± 0.0206	0.7322 ± 0.0304	0.5648 ± 0.0182	0.7906 ± 0.0374
3	BrainTokenGT	0.5330 ± 0.0339	0.5314 ± 0.0882	0.4663 ± 0.1734	0.5540 ± 0.1719
	WHGNCN	0.5954 ± 0.0438	0.5997 ± 0.0692	0.5958 ± 0.1046	0.6010 ± 0.1230
	SDEGCN	0.7103 ± 0.0271	0.6960 ± 0.0779	0.5448 ± 0.1533	0.7493 ± 0.1539
	SDE-HGNN	0.7726 ± 0.0361	0.7081 ± 0.0642	0.6987 ± 0.0973	0.7108 ± 0.1153
4	BrainTokenGT	0.5410 ± 0.0649	0.5741 ± 0.0500	0.4861 ± 0.0942	0.6045 ± 0.0715
	WHGNCN	0.6148 ± 0.0213	0.6079 ± 0.0739	0.5803 ± 0.1033	0.6175 ± 0.1330
	SDEGCN	0.7305 ± 0.0311	0.7095 ± 0.0202	0.5811 ± 0.0863	0.7545 ± 0.0181
	SDE-HGNN	0.7769 ± 0.0337	0.7496 ± 0.0409	0.6629 ± 0.0423	0.7795 ± 0.0695
5	BrainTokenGT	0.5758 ± 0.0244	0.5866 ± 0.0756	0.4709 ± 0.2040	0.6268 ± 0.1733
	WHGNCN	0.6153 ± 0.0363	0.6198 ± 0.0838	0.5753 ± 0.1385	0.6355 ± 0.1546
	SDEGCN	0.7153 ± 0.0234	0.7135 ± 0.0518	0.5287 ± 0.1178	0.7780 ± 0.1022
	SDE-HGNN	0.7808 ± 0.0354	0.7135 ± 0.0462	0.6833 ± 0.0767	0.7238 ± 0.0791
6	BrainTokenGT	0.5489 ± 0.0416	0.5649 ± 0.0269	0.4973 ± 0.0798	0.5885 ± 0.0147
	WHGNCN	0.6312 ± 0.0363	0.6506 ± 0.0471	0.5182 ± 0.1978	0.6965 ± 0.1216
	SDEGCN	0.7335 ± 0.0265	0.7148 ± 0.0393	0.5345 ± 0.1181	0.7780 ± 0.0781
	SDE-HGNN	0.7772 ± 0.0297	0.7255 ± 0.0317	0.6785 ± 0.0367	0.7417 ± 0.0511

Experiments and Results

We evaluate the proposed SDE-HGNN framework along four aspects: (i) longitudinal disease progression prediction under varying follow-up lengths on the OASIS-3 dataset; (ii) diagnostic classification on the ADNI dataset; (iii) ablation studies to analyze the contributions of key model components; and (iv) saliency visualization to assess model interpretability.

Datasets. We conduct experiments on two publicly available longitudinal neuroimaging datasets: OASIS-3¹⁶ and ADNI¹⁷. **OASIS-3 cohort:** The OASIS-3 cohort contains 747 subjects, including 193 progressive subjects and 554 stable subjects. Each subject contributes up to six irregular longitudinal visits, which are mapped to cohort-mean follow-up months: baseline, 34, 62, 74, 81, and 93 months. The irregular intervals between visits make this dataset particularly suitable for evaluating continuous-time disease progression models. **ADNI cohort:** The ADNI cohort includes 289 subjects (135 healthy controls, 100 MCI, and 54 AD). We evaluate three binary diagnostic tasks: HC vs. AD, HC vs. MCI, and MCI vs. AD.

Experimental Setup. For both datasets, rs-fMRI scans were preprocessed using the standard fMRIPrep pipeline¹⁸,

Table 2. Classification performance for different methods on ADNI dataset.

Tasks	Methods	AUC	Accuracy	Sensitivity	Specificity
HC vs. AD	DGCNN	0.5817 ± 0.1661	0.6797 ± 0.0993	0.3321 ± 0.2983	0.7733 ± 0.1111
	DwHGNCN	0.6312 ± 0.0362	0.6195 ± 0.0372	0.4653 ± 0.0635	0.7658 ± 0.0897
	BrainTokenGT	0.5770 ± 0.1119	0.5932 ± 0.0844	0.5222 ± 0.2603	0.6138 ± 0.1613
	WHGCN	0.6039 ± 0.1126	0.5453 ± 0.1298	0.5333 ± 0.3943	0.5551 ± 0.3273
	HyperGALE	0.6102 ± 0.0183	0.6769 ± 0.0625	0.4779 ± 0.0724	0.7872 ± 0.0729
	SDEGCN	0.6504 ± 0.0435	0.7141 ± 0.0225	0.4291 ± 0.1957	0.8296 ± 0.0895
	HGST	0.6036 ± 0.1163	0.6317 ± 0.0908	0.3882 ± 0.1122	0.7576 ± 0.1515
	SDE-HGNN	0.6989 ± 0.1008	0.6770 ± 0.0530	0.5382 ± 0.1101	0.7333 ± 0.1032
HC vs. MCI	DGCNN	0.5421 ± 0.1862	0.6308 ± 0.1376	0.4071 ± 0.2405	0.6913 ± 0.1844
	DwHGNCN	0.5876 ± 0.0087	0.6277 ± 0.0038	0.4433 ± 0.0522	0.6335 ± 0.0528
	BrainTokenGT	0.5628 ± 0.0654	0.5421 ± 0.0779	0.5130 ± 0.0748	0.5664 ± 0.1267
	WHGCN	0.5674 ± 0.0563	0.5421 ± 0.0887	0.4846 ± 0.3149	0.6375 ± 0.2860
	HyperGALE	0.5733 ± 0.0251	0.5953 ± 0.0152	0.4645 ± 0.0627	0.6638 ± 0.0142
	SDEGCN	0.5948 ± 0.0740	0.5915 ± 0.0313	0.3000 ± 0.2588	0.8074 ± 0.1596
	HGST	0.5639 ± 0.1513	0.6072 ± 0.1008	0.4154 ± 0.0987	0.6739 ± 0.2219
	SDE-HGNN	0.6241 ± 0.0480	0.6468 ± 0.0478	0.5500 ± 0.1140	0.7185 ± 0.0763
MCI vs. AD	DGCNN	0.5295 ± 0.1633	0.6414 ± 0.1012	0.3786 ± 0.2087	0.7117 ± 0.1432
	DwHGNCN	0.5325 ± 0.0076	0.6100 ± 0.0073	0.4142 ± 0.0575	0.6767 ± 0.0032
	BrainTokenGT	0.5372 ± 0.0993	0.5116 ± 0.0834	0.4964 ± 0.2447	0.5193 ± 0.1782
	WHGCN	0.5595 ± 0.0795	0.5746 ± 0.2189	0.3714 ± 0.3452	0.6231 ± 0.3628
	HyperGALE	0.5682 ± 0.0823	0.6174 ± 0.0526	0.3587 ± 0.0263	0.7342 ± 0.0198
	SDEGCN	0.5274 ± 0.0683	0.5460 ± 0.1059	0.4018 ± 0.4537	0.6200 ± 0.4057
	HGST	0.5349 ± 0.0948	0.6233 ± 0.2016	0.3766 ± 0.2313	0.7019 ± 0.1522
	SDE-HGNN	0.5873 ± 0.1414	0.6495 ± 0.0086	0.2455 ± 0.2909	0.8200 ± 0.1600

including slice-timing correction, MCFLIRT-based motion correction, and spatial normalization to the MNI152 template. To further reduce motion artifacts, ICA-AROMA¹⁹ was applied, followed by spatial smoothing with a 6 mm FWHM Gaussian kernel. The cortex was parcellated using the Schaefer-100 atlas²⁰, yielding 100 regions of interest (ROIs). ROI-level BOLD time series were extracted and used to construct node features for hypergraph modeling. To prevent data leakage and ensure predictive validity, only longitudinal scans prior to the point of clinical conversion were used for progressive subjects.

Functional connectivity representations were derived from the reconstructed ROI signals produced by the SDE module. Hypergraphs were constructed at each visit using a KNN strategy based on pairwise distances between ROI features. The number of neighbors K was set to 10. The proposed model was implemented in PyTorch and trained using the Adam optimizer. The learning rate, hidden dimensions, and regularization coefficients were selected via validation on the training folds. All experiments were conducted using five-fold cross-validation with identical stratified subject-level splits (6:2:2 ratio), and the reported results correspond to the average performance across folds. Performance is measured using the following metrics: area under the ROC curve (AUC), accuracy, sensitivity, and specificity.

Comparison with Competing Methods. We compare SDE-HGNN with both cross-sectional and longitudinal baselines. Cross-sectional baselines include DGCNN²¹, DwHGNCN¹⁰, HyperGALE¹¹, HGST¹². Longitudinal baselines include Brain-TokenGT⁶, WHGCN¹³, SDEGCN⁸. These baselines cover a range of graph and hypergraph neural network approaches for brain connectome analysis.

Table 3. Ablation results for temporal modeling and sparsity modules on the OASIS-3 dataset (progressive vs. stable classification with six time points).

Methods	AUC	Accuracy	Sensitivity	Specificity
HGNN+RNN	0.7328 \pm 0.0370	0.6760 \pm 0.0461	0.6078 \pm 0.2949	0.7001 \pm 0.1526
HGNN+ODE	0.7519 \pm 0.0414	0.7161 \pm 0.0722	0.6269 \pm 0.0216	0.7472 \pm 0.0941
SDE-HGNN (w/o Sparsity)	0.7556 \pm 0.0364	0.7161 \pm 0.0670	0.6069 \pm 0.1510	0.7541 \pm 0.1365
SDE-HGNN (Full)	0.7772 \pm 0.0297	0.7255 \pm 0.0317	0.6785 \pm 0.0367	0.7417 \pm 0.0511

Table 1 reports progression prediction results on OASIS-3 under varying numbers of longitudinal visits. SDE-HGNN consistently achieves the best performance across all settings. The performance gap becomes more pronounced as the number of visits increases, demonstrating the effectiveness of SDE-based continuous-time modeling in capturing longitudinal disease dynamics. In addition, the hypergraph formulation enables the model to capture higher-order interactions among multiple brain regions, leading to stronger performance even when only a small number of visits are available. Table 2 reports diagnostic classification results on ADNI. While the OASIS-3 experiments primarily evaluate longitudinal modeling capability, the ADNI experiments emphasize spatial representation learning. Across all diagnostic tasks, SDE-HGNN achieves the highest AUC and accuracy. In particular, the model shows clear advantages in the clinically challenging early-stage scenarios (HC vs. MCI and MCI vs. AD), indicating that the hypergraph representation effectively captures subtle multi-region functional abnormalities.

Ablation Studies. To assess the contribution of key components in SDE-HGNN, we conduct ablation studies on OASIS-3 by modifying the temporal evolution strategy and the sparsity mechanism. As shown in Table 3, two observations can be made. First, replacing the SDE-driven temporal evolution with a discrete-time RNN or deterministic ODE leads to a noticeable performance drop. This indicates that continuous-time stochastic modeling is important for capturing subject-specific variability in irregular longitudinal trajectories. Second, removing the sparsity regularization terms (\mathcal{L}_s , \mathcal{L}_e) also reduces performance. This suggests that the interpretability mechanism not only provides explanations but also acts as an effective regularizer that suppresses redundant connectivity patterns, thereby improving predictive performance.

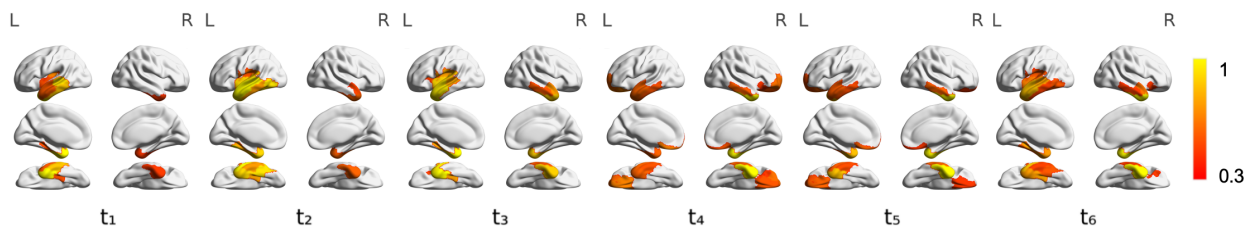


Figure 2. Longitudinal visualization of salient ROIs in the progressive group across six follow-up visits. Color indicates regional importance (yellow: higher; red: lower) among the top-20 ROIs at each time point.

Interpretation Analysis. To examine the clinical relevance of the learned representations, we visualize the top-20 salient ROIs for progressive subjects across six follow-up visits on the OASIS-3 dataset (Fig. 2). The visualization reveals a clear temporal evolution of important regions. Early visits consistently highlight the parahippocampal cortex, a well-established early biomarker of AD^{22,23}. At later stages, salient regions expand toward prefrontal and temporo-parietal cortices, consistent with the posterior-to-anterior spread of tau pathology described in Braak staging^{24,25}. These findings indicate that SDE-HGNN captures temporally evolving functional reorganization associated with AD progression rather than producing static importance patterns.

To further analyze connectivity changes, we examine the learned hyperedge importance probabilities and perform two-sample t -tests to identify statistically significant connectivity differences between stable and progressive groups on OASIS-3. Fig. 3 visualizes top-30 discriminative connections across six longitudinal time points. ROIs are grouped into seven large-scale functional networks based on the Schaefer100 (7-network) parcellation: visual (VIS), somato-motor (SMN), dorsal attention (DAN), ventral attention (VAN), limbic (LIM), frontoparietal control (CON), and default mode network (DMN). Across all visits, the most discriminative connections primarily involve the DAN, DMN,

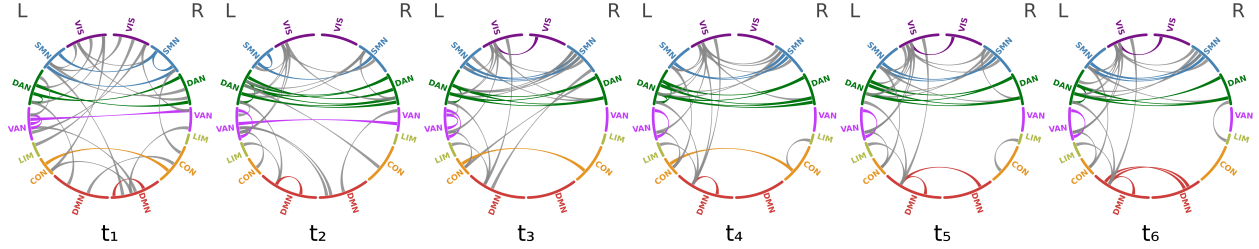


Figure 3. Top-30 discriminative functional connections between stable and progressive groups across six longitudinal time points (t_1 – t_6), identified via FDR-corrected two-sample t -tests ($p < 0.05$) on learned hyperedge importance probabilities. ROIs are grouped into seven large-scale neural systems based on the Schaefer100 (7-network) parcellation: visual (VIS), somatomotor (SMN), dorsal attention (DAN), ventral attention (VAN), limbic (LIM), frontoparietal control (CON), and default mode network (DMN). The intra-network connections are colored by their respective net-

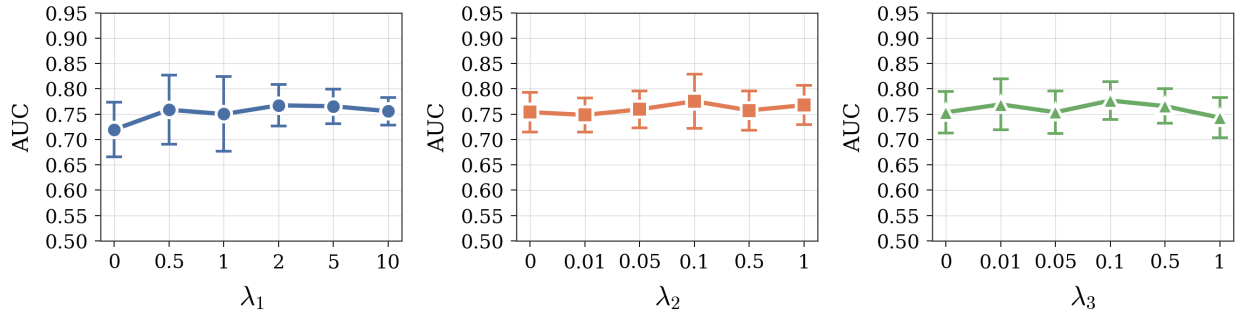


Figure 4. Sensitivity analysis of three loss weighting hyperparameters.

and SMN. Notably, interactions between DAN and DMN appear even at baseline, suggesting that early disruption of these opposing systems may serve as an early functional marker of AD. As disease progresses, connectivity differences increasingly involve prefrontal and temporo-parietal regions, consistent with known disease progression patterns.

Hyperparameter Sensitivity Analysis. We analyze the sensitivity of model performance to the three loss weighting parameters in Eq. (12): λ_1 (mutual information loss), λ_2 (ℓ_1 sparsity regularization), λ_3 (entropy regularization). For each parameter, we vary its value across six levels while fixing the remaining parameters at their optimal settings. Fig. 4 reports the resulting AUC values. Across all three parameters, we observe an inverted-U trend, where performance improves as the parameter increases from a small value, peaks at an intermediate value, and gradually decreases for larger values. The best performance is obtained at: $\lambda_1 = 2$, $\lambda_2 = 0.1$, and $\lambda_3 = 0.1$. These results indicate that moderate regularization provides the best balance between feature selection and predictive performance.

Conclusion

In this work, we propose an SDE-driven spatio-temporal hypergraph neural network learning framework (SDE-HGNN) for modeling irregular longitudinal brain connectomes in Alzheimer’s disease. By integrating continuous-time temporal modeling with higher-order hypergraph representations, the proposed method captures both disease progression dynamics and coordinated multi-region functional interactions beyond conventional pairwise connectivity. Extensive experiments on the OASIS-3 and ADNI datasets demonstrate that SDE-HGNN achieves robust performance across varying numbers of time points while generalizing to both longitudinal progression prediction and cross-sectional diagnosis. In addition, the sparsity-based importance learning mechanism identifies salient ROIs and connectivity patterns associated with disease progression, providing interpretable insights into disease-related brain network changes. These results highlight the value of jointly modeling temporal continuity and higher-order connectivity in irregular neuroimaging data. Moreover, the proposed framework offers a principled way to handle heterogeneous longitudinal observations in clinical studies. Future work will extend this framework to multimodal neuroimaging integration and larger clinical cohorts to further improve the characterization of disease trajectories and support data-driven clinical decision-making.

Acknowledgments

This work was supported in part by NIH (R01LM013519, RF1AG077820), NSF (IIS-2319451, MRI-2215789), DOE (DE-SC0025801), and Lehigh University (CORE and RIG).

References

1. Jack CR, Knopman DS, Jagust WJ, Shaw LM, Aisen PS, Weiner MW, et al. Hypothetical model of dynamic biomarkers of the Alzheimer's pathological cascade. *The Lancet Neurology*. 2010;9(1):119-28.
2. Logothetis NK. What we can do and what we cannot do with fMRI. *Nature*. 2008;453(7197):869-78.
3. Smith S. Overview of fMRI analysis. *The British journal of radiology*. 2004;77:S167-75.
4. Bessadok A, Mahjoub MA, Rekik I. Graph neural networks in network neuroscience. *IEEE Transactions on Pattern Analysis and Machine Intelligence*. 2022;45(5):5833-48.
5. Tong W, Li YX, Zhao XY, Chen QQ, Gao YB, Li P, et al. fMRI-based brain disease diagnosis: A graph network approach. *IEEE Transactions on Medical Robotics and Bionics*. 2023;5(2):312-22.
6. Dong Z, Wu Y, Xiao Y, Chong JSX, Jin Y, Zhou JH. Beyond the snapshot: Brain tokenized graph transformer for longitudinal brain functional connectome embedding. In: *International Conference on Medical Image Computing and Computer-Assisted Intervention*. Springer; 2023. p. 348-57.
7. Han K, Yang Y, Huang Z, Kan X, Guo Y, Yang Y, et al. Brainode: Dynamic brain signal analysis via graph-aided neural ordinary differential equations. In: *IEEE EMBS International Conference on Biomedical and Health Informatics*. IEEE; 2024. p. 1-8.
8. Zhou H, Zhou R, Liu Y, Zhao K, Shen L, Chen BY, et al. Uncovering alzheimer's disease progression via SDE-based spatio-temporal graph deep learning on longitudinal brain networks. *arXiv preprint arXiv:250921735*. 2025.
9. Mahmud AI, Suleiman AB, Yahaya U. Modelling functional brain aging in Alzheimer's disease using neural ODEs on rsfMRI graphs. *International Journal of Research Publication and Reviews*. 2025;6(7):2482-8.
10. Wang J, Li H, Qu G, Cecil KM, Dillman JR, Parikh NA, et al. Dynamic weighted hypergraph convolutional network for brain functional connectome analysis. *Medical image analysis*. 2023;87:102828.
11. Arora M, Jain CS, Baru LB, Dadi K, et al. Hypergale: Asd classification via hypergraph gated attention with learnable hyperedges. In: *2024 International Joint Conference on Neural Networks (IJCNN)*. IEEE; 2024. p. 1-8.
12. Han X, Lei M, Li J. Hypergraph-based semantic and topological self-supervised learning for brain disease diagnosis. *Pattern Recognition*. 2026;169:111921.
13. Hao X, Li J, Ma M, Qin J, Zhang D, Liu F, et al. Hypergraph convolutional network for longitudinal data analysis in Alzheimer's disease. *Computers in Biology and Medicine*. 2024;168:107765.
14. De Brouwer E, Simm J, Arany A, Moreau Y. GRU-ODE-Bayes: Continuous modeling of sporadically-observed time series. *Advances in neural information processing systems*. 2019;32.
15. Ying Z, Bourgeois D, You J, Zitnik M, Leskovec J. Gnnexplainer: Generating explanations for graph neural networks. *Advances in neural information processing systems*. 2019;32.
16. Marcus DS, Fotenos AF, Csernansky JG, Morris JC, Buckner RL. Open access series of imaging studies: longitudinal MRI data in nondemented and demented older adults. *Journal of cognitive neuroscience*. 2010;22(12):2677-84.
17. Mueller SG, Weiner MW, Thal LJ, Petersen RC, Jack C, Jagust W, et al. The Alzheimer's disease neuroimaging initiative. *Neuroimaging Clinics*. 2005;15(4):869-77.
18. Esteban O, Markiewicz CJ, Blair RW, et al. fMRIPrep: a robust preprocessing pipeline for functional MRI. *Nature Methods*. 2019;16(1):111-6.
19. Pruim RH, Mennes M, van Rooij D, et al. ICA-AROMA: A robust ICA-based strategy for removing motion artifacts from fMRI data. *NeuroImage*. 2015;112:267-77.
20. Schaefer A, Kong R, Gordon EM, Laumann TO, Zuo XN, Holmes AJ, et al. Local-global parcellation of the human cerebral cortex from intrinsic functional connectivity. *Cerebral cortex*. 2018;28(9):3095-114.
21. Zhao K, Duka B, Xie H, Oathes DJ, Calhoun V, Zhang Y. A dynamic graph convolutional neural network framework reveals new insights into connectome dysfunctions in ADHD. *NeuroImage*. 2022;246:118774.
22. Echávarri C, Aalten P, Uylings HB, Jacobs H, Visser PJ, Gronenschild E, et al. Atrophy in the parahippocampal gyrus as an early biomarker of Alzheimer's disease. *Brain Structure and Function*. 2011;215(3):265-71.

23. Van Hoesen GW, Augustinack JC, Dierking J, Redman SJ, Thangavel R. The parahippocampal gyrus in Alzheimer's disease: clinical and preclinical neuroanatomical correlates. *Annals of the new York Academy of Sciences*. 2000;911(1):254-74.
24. Braak H, Alafuzoff I, Arzberger T, Kretschmar H, Del Tredici K. Staging of Alzheimer disease-associated neurofibrillary pathology using paraffin sections and immunocytochemistry. *Acta neuropathologica*. 2006;112(4):389-404.
25. Vogel JW, Young AL, Oxtoby NP, Smith R, Ossenkoppele R, Strandberg OT, et al. Four distinct trajectories of tau deposition identified in Alzheimer's disease. *Nature medicine*. 2021;27(5):871-81.